INVESTIGATION ON THE DISCRETIZATION OF THE REALISTIC IRREGULAR WAVE GENERATION REGION THROUGH THE WAVEMIMO METHODOLOGY

M. da S. Paiva[a],
A. P. G. Mocellin[b],
A. H. da S. Koch[c],
P. H. Oleinik[d],
L. A. Isoldi[e],
and B. N. Machado[f]

Universidade Federal do Rio Grande do Sul, Campus do Vale - Porto Alegre, RS, Brasil.
[a]mayconpaiva@furg.br
[b]ana.mocellin@ufrgs.br
Universidade Federal do Rio Grande do Sul, Campus Litoral Norte - Tramandaí, RS, Brasil.
[c]augusto.koch@ufrgs.br
[f]bianca.machado@ufrgs.br
Universidade Federal do Rio Grande, Campus Carreiros - Rio Grande, RS, Brasil.
[d]phelype.oleinik@gmail.com
[e]liercioisoldi@furg.br

Received: Feb 07, 2023
Reviewed: Feb 25, 2023
Accepted: Feb 27,2023

ABSTRACT

Aiming to contribute to the research related to the sea wave energy conversion, the present paper approaches an investigation of the discretization used in the region of imposition of the prescribed velocity boundary condition, which is necessary for the WaveMIMO methodology. This methodology is employed for the numeric generation of irregular waves based on realistic sea state data. These data (obtained from TOMAWAC software in the present study) are treated to obtain orbital profiles of wave propagation velocity, which are imposed as boundary conditions on the wave channel. In this study, the realistic data considered refers to a point close to the Molhes da Barra, located on the coast of the municipality of Rio Grande, Rio Grande do Sul, Brazil. The numerical simulations were performed in Fluent, a computational fluid dynamics (CFD) software based on the finite volume method (FVM). The volume of fluid (VOF) multiphase model was used on the treatment of the water-air interface. Free surface elevation data obtained when the region of imposition of the prescribed velocity boundary condition was subdivided into 8, 11 and 14 segments were compared. The results found show that the 14 segments discretization represents more precisely the free surface elevation of irregular waves.

Keywords: waveMIMO methodology; realistic sea state; wave energy, computational modeling; irregular waves

NOMECLATURE

A	wave amplitude, m
C_1	linear damping coefficient, s^{-1}
C_2	quadratic damping coefficient m^{-1}
$\vec{g}$	gravity acceleration vector, m/s²
h	water depth, m
H_{max}	maximum height
H_s	significant wave height
I	counter variable
k	wave number, m^{-1}
k_x	component horizontal of the wave number vector, m^{-1}
k_z	component vertical of the wave number vector, m^{-1}
MAE	mean absolute error, m
N	directional spectrum of wave action density, m²/Hz/rad
n	total amount of data
O	numerical values from Fluent, m
p	static pressure, Pa
P	reference values from TOMAWAC, m
Q	source term, m²/rad
RMSE	root mean square error, m
S	damping sink term
T	wave period, s
t	time, s
T_m	mean period of realistic waves, s
u	horizontal component of the velocity propagation of the wave
$\vec{v}$	velocity vector, m/s

V	fluid velocity module at the analyzed point, m/s
w	vertical component of the velocity propagation of the wave
x	horizontal position of the coordinate system, m
x_s	horizontal position of the start of the numerical beach, m
x_e	horizontal position of the end of the numerical beach, m
z	vertical position of the coordinate system, m
z_{fs}	vertical position of the free surface, m
z_b	vertical positions of the bottom, m

Greek symbols

α	volumetric fraction
α_{water}	volume fraction of water phase
α_{air}	volume fraction of air phase
η	free surface elevation
λ	wavelength, m
μ	viscosity, kg/m.s
ρ	density, kg/m³
$\bar{\bar{\tau}}$	stress tensor, Pa
ω	angular wave frequency, Hz

1. INTRODUCTION

The current global energy crisis reinforces the need to explore new energy sources, especially renewable ones, which are dissociated from greenhouse gas emissions. According to Adesanya et al. (2020), the negative environmental aspects of generating energy from fossil fuels, and the prospect of inevitable depletion of these reserves, encourage countries and regions to explore and integrate renewable resources into their energy matrices.

In concordance with it, Hernández-Fontes et al. (2020) point to ocean energy resources as an alternative to fossil fuels, either on a large scale, in regions with high availability of resources, or on a smaller scale, covering the basic energy needs of small towns located in coastal regions. Among these resources, there is the energy contained in sea waves which, according to Espindola and Araújo (2017), in Brazil have the potential of approximately 89.97 GW, being the southern region the one with the highest energy potential.

The sea wave energy can be extracted through wave energy converter (WEC) devices that, according to Pecher and Kofoed (2017), can be classified as: oscillating water column (OWC), with a fixed or floating structure; oscillating bodies, with floating or submerged structures; and overtopping, with a fixed or floating structure. However, this classification do not cover all the operational principles that a WEC device might present, such as the submerged horizontal plate (Seibt et al., 2017). It is also important to highlight that WECs have been studied and developed both in the experimental and numerical fields.

Regarding to numerical studies, Machado et al. (2021) presented the WaveMIMO methodology, which allows numerical simulation of irregular waves based on realistic sea states data. In this methodology, the wave generation occurs through the imposition of discretized orbital velocity profiles, both horizontal and vertical, of wave propagation as boundary conditions based on realistic sea state data, thus allowing the numerical simulation of irregular waves that occur in nature.

The WaveMIMO Methodology can be employed in studies that evaluate the fluid dynamic behavior of WECs, as in Koch et al. (2022), who analyzed the available hydropneumatic power of a OWC device, when subjected to irregular realistic sea state data and when subjected to regular waves representative of that sea state; Hübner et al. (2022), who compared the fluid dynamic behavior of an overtopping under the incidence of realistic and regular representative irregular waves, considering points in three regions of the coast of Rio Grande do Sul. Moreover, in Maciel et al. (2021), the WaveMIMO Methodology was verified and validated for the generation of regular waves, by comparing the numerical results obtained with experimental ones.

Aiming to contribute to the improvement of the WaveMIMO methodology (Machado et al., 2021), the present study investigates the discretization used in the region of imposition of the prescribed velocity boundary conditions. Thereunto, it was considered realistic sea state data referring to 09/11/2018 at the point of geographic coordinates -52°4' 45.08"W, -32°11' 24.92"S, located at 171.06 m away from Molhes da Barra, on the coast of the Rio Grande (RG) municipality, in the Rio Grande do Sul (RS) state.

2. MATHEMATICAL AND COMPUTATIONAL MODELING

To carry out the study, numerical simulations of wave generation will be performed in a wave channel using Fluent 2020 R1, which is a computational fluid dynamics (CFD) software based on the finite volume method (FVM) (Maliska, 2004). The multiphase volume of fluid (VOF) model, proposed by Hirt and Nichols (1981), is used to treat the phase interface.

To represent the phases considered in this study, which are water and air, the concept of volumetric fraction (α) is necessary. It is important to emphasize that the sum of the phases in each control volume must be unitary. Thus, as there are two phases considered in this study, each computational cell might be in three different states: containing only the water phase, in this case $\alpha_{water} = 1$; containing only the air phase, where

$\alpha_{air} = 1$; or containing the interface of the two phases, in this case $\alpha_{water} + \alpha_{air} = 1$. Furthermore, as the VOF is used in immiscible fluids, that is, fluids that do not mix, it is valid that $\alpha_{water} = 1 - \alpha_{air}$.

In the VOF model, a single set of equations is solved. Thus, the volumetric fraction is considered along the computational domain through the transport equation. Therefore, according to Versteeg and Malalasekera (2007), the model is composed of three equations: continuity; the volumetric fraction transport; and the Navier-Stokes equation for a water-air mixture, respectively, given by:

$$\frac{\partial(\rho)}{\partial t} + \nabla.(\rho\vec{v}) = 0 \quad (1)$$

$$\frac{\partial(\alpha)}{\partial t} + \nabla.(\alpha\vec{v}) = 0 \quad (2)$$

$$\frac{\partial}{\partial t}(\rho\vec{v}) + \nabla.(\rho\vec{v}).\vec{v} = -\nabla.p + \nabla.(\mu\bar{\bar{\tau}}) + \rho\vec{g} + S \quad (3)$$

Moreover, S refers to the numerical beach tool, given by (Lisboa et al., 2017):

$$S = -\left[C_1\rho V + \frac{1}{2}C_2\rho|V|V\right]\left(1 - \frac{z - z_{fs}}{z_b - z_{fs}}\right)\left(\frac{x - x_s}{x_e - x_s}\right)^2 \quad (4)$$

where, the damping coefficients, following the recommendations of Lisboa et al. (2017), are defined as $C_1 = 20$ s^{-1} and $C_2 = 0$ m^{-1}.

2.1 WaveMIMO Methodology

The generation of realistic irregular waves in the Fluent software occurs through the imposition of discrete transient data of the orbital propagation velocities of the sea state waves in the horizontal (u) and vertical (w) directions as prescribed velocity boundary conditions. Thus, the WaveMIMO methodology, presented in Machado et al. (2021), which can treat realistic sea state data from the TOMAWAC (TELEMAC-based Operational Model Addressing Wave Action Computation) spectral model to obtain the orbital velocity profiles.

According to Awk (2017), the TOMAWAC data are obtained from the solution of Eq. (5), which represents the general situation of wave propagation in an unstable and inhomogeneous medium, where the wave action density (N) is conserved in the source term (Q):

$$\frac{\partial N}{\partial t} + \frac{\partial(\dot{x}N)}{\partial x} + \frac{\partial(\dot{z}N)}{\partial z} + \frac{\partial(\dot{k}_x N)}{\partial k_x} + \frac{\partial(\dot{k}_z N)}{\partial k_z} = Q(k_x, k_z, x, z, t) \quad (5)$$

After obtaining the sea state data, the wave spectrum is transformed into a free surface elevation by means the procedure proposed and validated by Oleinik et al. (2021). Thereunto, the generated phase spectrum and the inverse Fourier transform are used, allowing to approximate the spectral data by a finite sum of monochromatic waves. Airy's linear wave theory (Airy, 1845) allows describing, individually, the elevation of the free surface (η) of monochromatic waves (Dean and Dalrymple, 1991):

$$\eta = A\cos(kx - \omega t) \quad (6)$$

which allows the orbital velocity profiles of wave propagation in the horizontal (u) and vertical (w) directions to be obtained, respectively, by (Dean and Dalrymple, 1991):

$$u = Agk\frac{\cosh(kz + kh)}{\omega\cosh(kh)}\cos(kx - \omega t) \quad (7)$$

$$w = Agk\frac{\sinh(kz + kh)}{\omega\cosh(kh)}\sin(kx - \omega t) \quad (8)$$

Moreover, the wave number and angular frequency are given, respectively, by:

$$k = \frac{2\pi}{\lambda} \quad (9)$$

$$\omega = \frac{2\pi}{T} \quad (10)$$

2.2 Realistic Sea State Data

As mentioned, the realistic sea state data addressed in this study refer to a point located near Molhes da Barra, in the municipality of Rio Grande, in the south region of the Rio Grande do Sul state. Realistic data of significant height (H_s) and mean period (T_m) referring to the selected point were analyzed to determine the most frequent sea state. Then, aiming to establish the representative regular waves of this sea state, the wavelength (λ) was calculated. Thereunto, the dispersion relation was used (Dean e Dalrymple, 1991):

$$\omega^2 = g\,k\tanh(kh) \quad (11)$$

Figure 1 presents the bivariate histogram that relates the combinations of H_s and T_m of the waves at the analyzed point.

Thus, the characteristics of regular waves representative of the sea state, which are used for spatial discretization of the computational domain, are: height $H_s = 1.14$ m; length $\lambda = 31.50$ m; mean period $T_m = 4.50$ s; and depth $h = 13.29$ m. Furthermore, it is highlighted that h refers to the depth found at the location of the point selected for the study.

3. PROBLEM DESCRIPTION

The aim of the present study is to carry out an investigation regarding the discretization of the numerical wave channel region where the prescribed velocity boundary condition is imposed. The study is justified because in the application of the WaveMIMO methodology (Machado et al., 2021), the insertion of transient discrete data of the orbital wave propagation velocities occurs through the subdivision of this region into straight line segments.

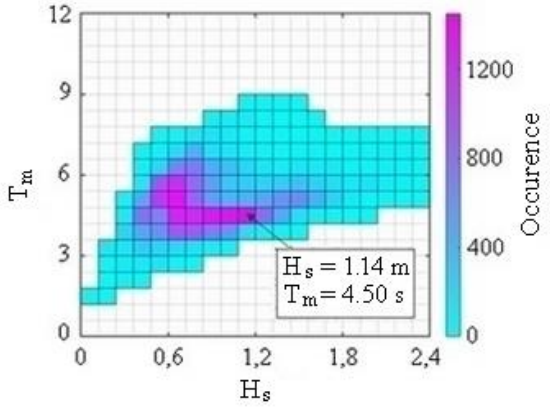

Figure 1. Histogram of recurrence of waves relating H_s and T_m.

For the investigation of the discretization to be adopted, the present study evaluates the subdivision into 14 segments presented in Machado et al. (2021) and proposes two other approaches, which consist of using the maximum height (H_{max}) and the significant height (H_s) of the waves as a parameter. It is worth to note that H_{max} is given by the module of the largest crest or largest trough found in the free surface elevation data from the TOMAWAC spectral model during the analyzed period, thus, in this case $H_{max} = 1.6419$ m.

Thus, instead of fixing the number of segments used in the subdivision of the boundary condition imposition region, as done in Machado et al. (2021), it is proposed that a relationship be established between H_{max} or H_s with the depth (h) found in the studied region. Thereby, for each case studied, the imposition region will have a different number of segments, with length approximately equal to the maximum height (H_{max}) or the significant height (H_s) of the wave. Moreover, in the case where the recommendation of Machado et al. (2021) is employed, the length of the segments is $h/14$.

Figure 2 illustrates the cited approach applied for the subdivision of the region using the H_{max} parameter. It is highlighted that the subdivision occurs in the same way as that illustrated when the parameter is H_s or $h/14$.

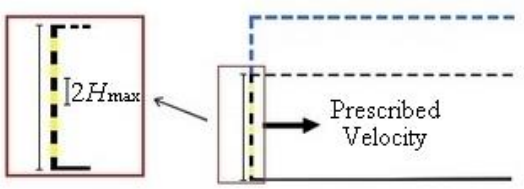

Figure 2. Subdivision of the boundary condition imposition region.

To determine the best tested case, a free surface elevation monitoring probe was used in the wave generation zone, i.e., at $x = 0$ m. The results obtained in the numerical simulations were compared, individually, with the free surface elevation that comes from the TOMAWAC spectral model. This comparison was made by calculating the averages mean absolute error (MAE) and root mean square error (RMSE) given, respectively, by (Chai and Draxler, 2014):

$$\mathrm{MAE} = \frac{\sum_{i=1}^{n} |O_i - P_i|}{n} \tag{11}$$

$$\mathrm{RMSE} = \sqrt{\frac{\sum_{i=1}^{n} (O_i - P_i)^2}{n}} \tag{12}$$

3.1 Computational Domain

The numerical wave channel has length $L = 171.06$ m, height $H = 16.00$ m and depth ranging from $h_1 = 13.29$ m, in the region of the selected point, to $h_2 = 10.54$ m, in the region close to the breakwater, reproducing the bathymetry found in the Molhes da Barra region of Rio Grande. Following the recommendation of Lisboa et al. (2017), the numerical beach region has a length of 2λ, i.e., $L_B = 63.00$ m. It is worth mentioning that the numerical beach, given by Eq. (4), dissipates the energy contained in the waves, thus avoiding the occurrence of their reflection, which would cause deviations in the free surface elevation. Finally, the illustration of the computational domain can be seen in Fig. 3, where WLR represents the water level at rest and lines r_1 and r_2 delimit the free surface region.

The computational domain was discretized through a stretched mesh, as in Gomes et al. (2012).

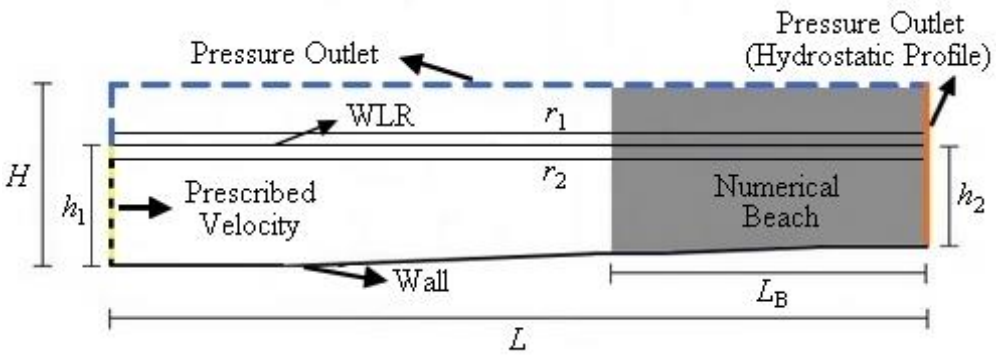

Figure 3. Illustration of the computational domain used.

Thus, the domain was vertically subdivided into three regions: the region containing only air, which was discretized into 20 computational cells; the free surface region, which contains the air-water interface, that was discretized into 40 cells; and the region containing only water, which was discretized into 60 computational cells. Horizontally, 50 computational cells per wavelength (λ) were used.

It is also noted that the free surface region has a different size for each analyzed case. This region is defined based on the size of the segments used for the discretization of the region of imposition of the prescribed velocity boundary conditions, being composed by one segment above and another below the WLR (see Fig. 3). Thus, when the parameters H_{max} and H_s are used, the region has the approximate length of, respectively, $2H_{max}$ and $2H_s$. Moreover, in the third case, when 14 segments are used, as recommended by Machado et al. (2021), each segment has length of 0.9496 m, that is, the total height of the free surface region is 1.8992 m.

The PISO (Pressure-Implicit with Splitting of Operators) scheme was used to solve the pressure-velocity coupling; and for the discretization of the pressure equation, the PRESTO (PREssure STaggering Option) scheme was employed. The first-order upwind discretization method was adopted to treat advective terms. Furthermore, it was considered that the flow is transient and occurs in the laminar regime. As for temporal discretization, a time step of $\Delta t = 0.05$ s was used, following the recommendation of Machado et al. (2021). Finally, regarding the total simulation time, 900 s of wave generation and propagation were considered.

4. RESULTS AND DISCUSSIONS

The free surface elevations obtained in numerical simulations of realistic irregular wave generation were compared to the free surface elevations derived from the TOMAWAC spectral model. Thus, it was possible to carry out a qualitative evaluation of the results. In Fig. 4 is presented the case in which H_{max} was used as parameter, thereby the region of imposition of the prescribed velocity boundary conditions was subdivided into 8 segments of 1.6616 m each. Figure 4 shows, as expected, that over the 900 s of numerical simulation, all waves are within the free surface region. It is also worth to recall that the lines r_1 and r_2, shown in Figs. 4, 5 and 6 delimit the free surface region.

In Figure 5, the comparison of the free surface elevation is presented for the case considering the parameter H_s, where the region of imposition of the boundary condition was subdivided into 11 segments of length 1.2086 m. As can be seen in Fig. 5, at the approximate time instants of $t = 170$ s, $t = 800$ s and $t = 895$ s, some crests and troughs of the irregular waves are outside the free surface region of the stretched mesh, i.e., are in less refined regions of the mesh. However, most of the generated waves are concentrated within the free surface region. This occurs because, in this case, the segments considered in the discretization of the boundary condition imposition region are smaller than H_{max}.

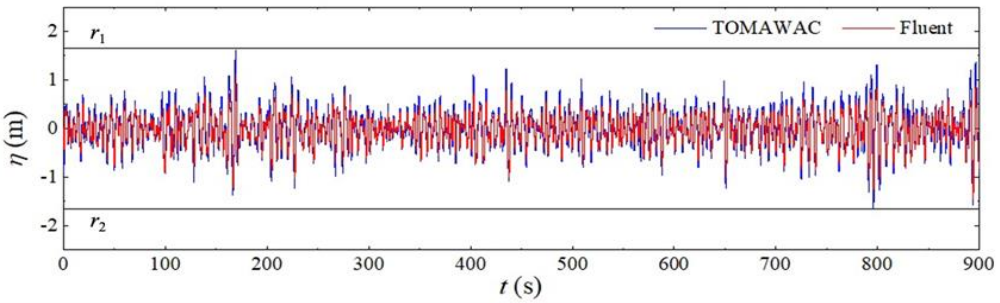

Figure 4. Comparison of free surface elevation for realistic irregular wave considering H_{max}.

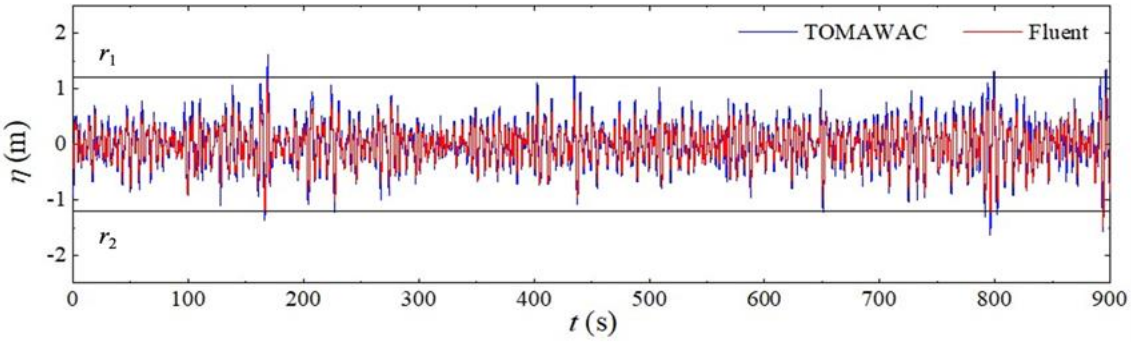

Figure 5. Comparison of free surface elevation for realistic irregular waves considering H_s.

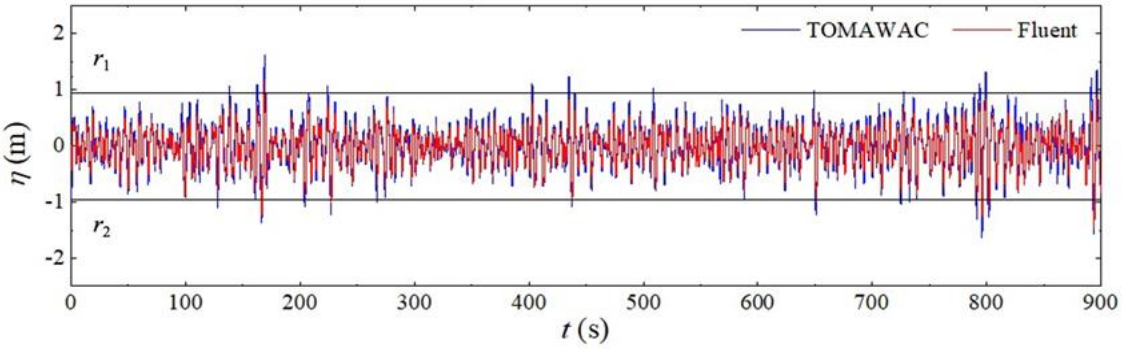

Figure 6. Comparison of free surface elevation for realistic irregular waves considering the recommendation of de Machado et al. (2021).

A similar behavior to that seen in Fig. 5, however, for other instants of time, can be observed in Fig. 6, which presents the results regarding the recommendation by Machado et al. (2021), where the boundary condition imposition region is subdivided into 14 segments of 0.9496 m.

Note that in the 3 cases analyzed, the realistic irregular waves present a similar behavior to that observed in the realistic data from the TOMAWAC spectral model. Thus, a quantitative analysis of the results is necessary. Thereunto, Table 1 presents the MAE and RMSE averages found for the evaluated cases along with the vertical dimension of the mesh elements, or computational cells, present in the free surface region for each case, allowing us to consider the mesh refinement.

Table 1 – Results for MAE and RMSE averages.

Number of Segments	Dimension of Mesh Elements (m)	MAE (m)	RMSE (m)
8	0.0831	0.1140	0.1485
11	0.0604	0.1116	0.1453
14	0.0475	0.1101	0.1434

The results in Table 1 indicate a gradual improvement as it increaser the discretization of the region where the boundary condition is imposed, i.e., in this study, the MAE and RMSE are directly proportional to the size of the segments used in the discretization of the inlet region. As can be seen in Table 1, the best evaluated case is the one subdivided into 14 segments of length 0.9496 m, where the free surface region is 1.8992 m long.

It is worth to highlight that, as well as in the other evaluated cases, the free surface region was vertically discretized into 40 computational cells, however, the case with 14 segments presents the greatest refinement since the mesh elements are smaller than the mesh elements used in the other cases. Also, since most of the elevation data is within the free surface region, it is computed more accurately.

5. CONCLUSION

Aiming to contribute to the improvement of the WaveMIMO methodology, employed for the generation of realistic irregular waves, the present study proposed two approaches for the discretization of the region of imposition of the prescribed velocity boundary condition, which relates the depth (h) with the parameters: maximum height (H_{max}) or significant height (H_s) of the waves. Furthermore, the subdivision of the region into 14 segments, recommended by Machado et al. (2021) when presenting the methodology, was also evaluated.

Based on the evaluations carried out, it was possible to determine that the best results were obtained when the boundary condition imposition region was subdivided into 14 segments, as done in

Machado et al. (2021). Moreover, it is noted that this is the case in which the free surface region, delimited during the process of generating the stretched mesh, has a greater refinement, which means it has smaller computational cells than the other tested cases, which may lead to greater accuracy of the results obtained.

This preliminary analysis motivates the realization of more detailed future investigations, among these, it is suggested: the definition of a stretched mesh recommendation for use in realistic irregular wave simulations, based in the characteristics of the representative regular waves of the sea state addressed, and that the mesh analysis is carried out considering other points along the Brazilian coast, thus enabling the analysis for different wave climates and depths.

ACKNOWLEDGEMENTS

A. P. G. M. and M. da S. P. thank the Brazilian Coordination for the Improvement of Higher Education Personnel – CAPES (Finance Code 001) for their master scholarship. A. H. da S. K. thank Brazilian National Council for Scientific and Technological Development – CNPq for his Scientific Initiation scholarship. L. A. I. thank CNPq for his Research Productivity grant, PQ1D (process: 309648/2021-1), and the Research Support Foundation of the State of Rio Grande do Sul – FAPERGS for the financial support through Programa Pesquisador Gaúcho – PqG (process: 21/2551-0002231-0).

REFERENCES

Airy, G. B., 1845, *Tides and Waves*, Encyclopaedia Metropolitana.

Adesanya, A.; Misra, S.; Maskeliunas, R.; Damasevicius, R., 2020, Prospects of ocean-based renewable energy for West Africa's sustainable energy future. Smart and Sustainable Built Environment. DOI: 10.1108/SASBE-05-2019-0066.

Awk, T., 2017, *TOMAWAC User Manual Version 7.2. 7.2.3*, The Telemac-Mascaret Consortium. URL: www.opentelemac.org.

Chai, T.; Draxler, R. R., 2014, Root mean square error (RMSE) or mean absolute error (MAE)? Arguments against avoiding RMSE in the literature. Geoscientific Model Development, v. 7. DOI: 10.5194/gmd-7-1247-2014.

Dean, R. G.; Dalrymple, R. A., 1991, *Water wave mechanics for engineers and scientists*, v. 2, World Scientific, Singapura, 353 p.

Espindola, R. L. e Araújo, A. M., 2017, Wave energy resource of Brazil: An analysis from 35 years of ERA-Interim reanalysis data. PLoS One, v. 12. DOI: 10.1371/journal.pone.0183501.

Gomes, M. N.; Isoldi, L. A.; Dos Santos, E. D.; Rocha, L. A. O., 2012, Análise de malhas para geração numérica de ondas em tanques, *VII Congresso Nacional de Engenharia Mecânica*, Associação Brasileira de Engenharia e Ciências Mecânicas. URL: http://repositorio.furg.br/handle/1/4995.

Hernández-Fontes, J. V.; Martínez, M. L.; Wojtarowski, A.; González-Mendoza, J. L.; Landgrave, R.; Silva, R., 2020, Is ocean energy an alternative in developing regions? A case study in Michoacan, Mexico. Journal of Cleaner Production, v. 266. DOI: 10.1016/j.jclepro.2020.121984.

Hirt, C. W.; Nichols, B. D., 1981, Volume of fluid (VOF) method for the dynamics of free boundaries. Journal of Computational Physics, 39, 201–225. DOI: 10.1016/0021-9991(81)90145-5.

Hubner, R. G.; Fragassa, C.; Paiva, M. S.; Oleinik, P. H.; Gomes, M. N.; Rocha, L. A. O.; Santos, E. D.; Machado, B. N.; Isoldi, L. A., 2022, Numerical Analysis of an Overtopping Wave Energy Converter Subjected to the Incidence of Irregular and Regular Waves from Realistic Sea States. Journal of Marine Science and Engineering, v. 10. DOI: 10.3390/jmse10081084.

Koch, A. H. S.; Paiva, M. S.; Monteiro, C. B.; Oleinik, P. H.; Isoldi, L. A.; Machado, B. N., 2022, Numerical Evaluation of the Hydropneumatic Power of the Oscillating Water Column Wave Energy Converter Submitted to Regular and Irregular Waves. Engineering Science & Technology, 32-43. DOI: 10.37256/est.3120221022.

Lisboa, R. C.; Teixeira, P. R.; Didier, E., 2017, Regular and irregular wave propagation analysis in a flume with numerical beach using a Navier-Stokes based model. Defect and Diffusion Forum, 372, 81-90. DOI: 10.4028/www.scientific.net/DDF.372.81.

Maliska, C. R., 2004, *Transferência de Calor e Mecânica dos Fluidos Computacional*, 2.ed, LTC - Livros Técnicos e Científicos, Rio de Janeiro, Brasil.

Machado, B. N.; Oleinik, P. H.; Kirinus, E. P.; Dos Santos, E. D.; Rocha, L. A. O.; Gomes, M. N.; Conde, J. M. P.; Isoldi, L. A., 2021, WaveMIMO methodology: numerical wave generation of a realistic sea state. Journal of Applied and Computational Mechanics, v. 7. DOI: 10.22055/jacm.2021.37617.3051.

Maciel, R. P.; Fragassa, C.; Machado, B. N.; Rocha, L. A. O.; Dos Santos, E. D.; Gomes, M. N.; Isoldi, L. A., 2021, Verification and Validation of a Methodology to Numerically Generate Waves Using Transient Discrete Data as Prescribed Velocity Boundary Condition. Journal of Marine Science and Engineering, v. 9. DOI: 10.3390/jmse9080896.

Oleinik, P. H.; Tavares, G. P.; Machado, B. N.; Isoldi, L. A., 2021, Transformation of Water WaveSpectra into Time Series of Surface Elevation. Earth, v. 2. DOI: 10.3390/earth2040059.

Pecher, A.; Kofoed, J. P., 2017, *Handbook of Ocean Wave Energy*, Springer Nature, Berlin.

Seibt, F. M.; Isoldi, L. A.; dos Santos, E. D.; Rocha, L. A. O., 2017, Study of The Effect of The

Relative Height on The Efficiency of a Submerged Horizontal Plate Type Wave Energy Converter Applying Constructal Design, in *XXXVIII Iberian Latin American Congress on Computational Methods in Engineering*, Florianópolis.

Versteeg, H.K.; Malalasekera, W., 2007, *An introduction to computational fluid dynamics: The finite volume method*, Pearson Education Limited, Harlow.